University of Nebraska - Lincoln
DigitalCommons@University of Nebraska - Lincoln

Mechanical & Materials Engineering Faculty Publications

Mechanical & Materials Engineering, Department of

2019

9R phase enabled superior radiation stability of nanotwinned Cu alloys via in situ radiation at elevated temperature

Cuncai Fan
Purdue University

Dongyue Xie
University of Nebraska-Lincoln, dxie5@unl.edu

Jin Li
Purdue University

Zhongxia Shang
Purdue University

Youxing Chen
University of North Carolina, Charlotte, ychen103@uncc.edu

See next page for additional authors

Follow this and additional works at: https://digitalcommons.unl.edu/mechengfacpub

 Part of the Mechanics of Materials Commons, Nanoscience and Nanotechnology Commons, Other Engineering Science and Materials Commons, and the Other Mechanical Engineering Commons

Fan, Cuncai; Xie, Dongyue; Li, Jin; Shang, Zhongxia; Chen, Youxing; Xue, Sichuang; Wang, Jian; Li, Meimei; El-Azab, Anter; Wang, Haiyan; and Zhang, Xinghang, "9R phase enabled superior radiation stability of nanotwinned Cu alloys via in situ radiation at elevated temperature" (2019). *Mechanical & Materials Engineering Faculty Publications*. 389.
https://digitalcommons.unl.edu/mechengfacpub/389

This Article is brought to you for free and open access by the Mechanical & Materials Engineering, Department of at DigitalCommons@University of Nebraska - Lincoln. It has been accepted for inclusion in Mechanical & Materials Engineering Faculty Publications by an authorized administrator of DigitalCommons@University of Nebraska - Lincoln.

Authors

Cuncai Fan, Dongyue Xie, Jin Li, Zhongxia Shang, Youxing Chen, Sichuang Xue, Jian Wang, Meimei Li, Anter El-Azab, Haiyan Wang, and Xinghang Zhang

This article is available at DigitalCommons@University of Nebraska - Lincoln: https://digitalcommons.unl.edu/mechengfacpub/389

University of Nebraska Lincoln
digitalcommons.unl.edu

9R phase enabled superior radiation stability of nanotwinned Cu alloys via *in situ* radiation at elevated temperature

Cuncai Fan,[1] Dongyue Xie,[2] Jin Li,[1]
Zhongxia Shang,[1] Youxing Chen,[3] Sichuang Xue,[1]
Jian Wang,[2] Meimei Li,[4] Anter El-Azab,[1,5]
Haiyan Wang,[1,6] and Xinghang Zhang[1]

1 School of Materials Engineering, Purdue University, West Lafayette, IN, 47907, USA
2 Nebraska Center for Materials and Nanoscience, University of Nebraska-Lincoln, Lincoln, NE, 68583-0857, USA
3 Department of Mechanical Engineering and Engineering Science, University of North Carolina, Charlotte, NC, 28223-0001, USA
4 Nuclear Engineering Division, Argonne National Laboratory, Argonne, IL, 60439, USA
5 School of Nuclear Engineering, Purdue University, West Lafayette, IN, 47907, USA
6 School of Electrical and Computer Engineering, Purdue University, West Lafayette, IN, 47907, USA

Corresponding author — X. Zhang, *email* xzhang98@purdue.edu

Abstract

Nanotwinned metals exhibit outstanding radiation tolerance as twin boundaries effectively engage, transport and eliminate radiation-induced defects. However, radiation-induced detwinning may reduce the radiation tolerance associated with twin

Published in *Acta Materialia* 167 (2019), pp 248–256.
doi 10.1016/j.actamat.2019.01.037
Copyright © 2019; published by Elsevier Ltd on behalf of Acta Materialia Inc. Used by permission.
Submitted 22 September 2018; revised 9 January 2019; accepted 23 January 2019; published 29 January 2019

boundaries, especially at elevated temperatures. Here we show, via *in-situ* Kr ion irradiation inside a transmission electron microscope, that 3 at. % Fe in epitaxial nanotwinned Cu ($Cu_{97}Fe_3$) significantly improves the thermal and radiation stability of nanotwins during radiation up to 5 displacements-per-atom at 200 °C. Such enhanced stability of nanotwins is attributed to a diffuse 9R phase resulted from the dissociation of incoherent twin boundaries in nanotwinned $Cu_{97}Fe_3$. The mechanisms for the enhanced stability of twin boundaries in irradiated nanotwinned alloys are discussed. The stabilization of nano-twins opens up opportunity for the application of nanotwinned alloys for aggressive radiation environments.

Keywords: Nanotwins, Radiation, Detwinning, 9R phase, Solute drag

1. Introduction

Energetic particle irradiation of metallic materials produces large amounts of point defects (interstitials and vacancies), which can further aggregate into extended defect clusters in the form of dislocation loops [1–5], stacking fault tetrahedrons (SFTs) [6–11] or cavities [12–23], resulting in microstructural evolution and degradation of mechanical properties [24–29]. It has been proposed that the radiation tolerance of materials can be significantly improved by using defect sinks [30–35]. Nanostructured materials contain abundant defect sinks and have shown enhanced radiation tolerance [27,36–39]. Grain boundaries (GBs) are one of the effective defect sinks [40], and nanograined (NG) materials show enhanced radiation tolerance compared with their coarse-grained (CG) counterparts as evidenced by fewer defects [41,42], reduced radiation hardening [43], stronger resistance to amorphization [44] and much less void swelling [14,45]. However, due to the high excess energy of conventional high-angle GBs, NG materials often suffer from poor thermal stability [46], and radiation-induced grain coarsening can occur even at room temperature [47]. Design of nanomaterials that can survive harsh radiation environments at elevated temperatures remains a major challenge [31,48].

Nanotwinned (NT) metals have raised significant interest due to their unique combination of remarkable mechanical properties [49–53] and superior thermal stability [54,55], as well as enhanced radiation tolerance [56–59]. *In-situ* studies have revealed that twin boundaries (TBs) can frequently interact with radiation-induced defects and tailor their formation and distribution [56,57,60–62]. For instance, fewer

defects are formed in NT Cu than in CG Cu under the same radiation conditions [57]. In addition, SFT, a notorious defect, can be destructed by interacting with TBs [56].

In NT metals with face centered cubic (FCC) structure, there are two major types of TBs: Σ3 {111} coherent twin boundaries (CTBs) and Σ3 {112} incoherent twin boundaries (ITBs) [63,64]. Extensive studies have shown that ITBs, containing arrays of Shockley partials, can migrate under irradiation [65], stress [66], high temperature [67] and electrical field [68]. As a result, detwinning occurs through ITB migration, decreases twin density, and compromises the performance of NT materials [69,70]. Therefore, to further improve the radiation tolerance of NT metals, it is of great significance to stabilize TBs, especially the highly mobile ITBs.

In this paper, we successfully synthesized epitaxial NT-$Cu_{97}Fe_3$ and compared its radiation response to that of NT-Cu by using *in situ* Kr^{++} irradiation at 200 °C inside a transmission electron microscope (TEM). The *in-situ* studies show that, in contrast to rapid detwinning in NT-Cu, the sharp ITBs in NT-$Cu_{97}Fe_3$ evolve into diffuse 9R phase and are highly stable against radiation at elevated temperatures. ITB migration velocity in NT-$Cu_{97}Fe_3$ is significantly lower than that in NT-Cu, lending experimental support for stabilizing NT structures via the introduction of certain solutes. *In-situ* studies also show that ITBs and CTBs in NT-$Cu_{97}Fe_3$ actively engage and eliminate radiation-induced defects.

2. Experimental methods

Highly-textured NT-Cu and NT-$Cu_{97}Fe_3$ alloy films, ~2 mm thick, were deposited on HF etched Si (110) substrates by using direct current magnetron sputtering technique at room temperature. Pure Cu (99.995%) and Fe (99.99%) targets were used for sputtering, and the chamber was evacuated to a base pressure ~ 5×10^{-8} torr prior to deposition. During deposition, ~1.2×10^{-3} torr Ar working pressure was used, and the deposition rate was controlled at ~0.6 nm/s. After depositions, the TEM specimens for irradiations were prepared by polishing, dimpling and low energy (3.5 keV) Ar ion milling. Subsequent heavy ion (1 MeV Kr^{++}) irradiations on the cross-sectional TEM samples were conducted in the Intermediate Voltage Electron Microscope

(IVEM) at Argonne National Laboratory, where an ion accelerator was attached to a Hitachi-9000 TEM microscope. More specific information regarding such *in-situ* heavy ion irradiation technique has been described elsewhere [71]. Before irradiation, the TEM specimens were annealed at 200 °C inside the IVEM column for 30 min. Then it was followed by Kr^{++} irradiations at 200 °C. During the irradiation, a CCD camera was utilized to capture videos at 15 frames/s.

The texture of as-deposited films was analyzed using an X-ray diffraction technique on a Panalytical Empyrean X'pert PRO MRD diffractometer with a Cu $K\alpha_1$ source. All the as-prepared and irradiated TEM samples were examined by a Thermo Fischer Scientific/ FEI Talos 200X analytical TEM with Super-X EDS detectors. The Stopping and Range of Ions in Matter (SRIM) simulation with Kinch-Pease method was used to estimate the radiation damage in unit of displacements-per-atom (dpa) [72,73]. As the Fe content is low in NT-$Cu_{97}Fe_3$, the radiation damage profile was simulated based on pure Cu. SRIM simulations calculated for pure Cu (Supplementary Fig. S1) show that ~ 99% of Kr ions have penetrated through TEM foils, leaving most radiation damage behind. The average ion dose rate was ~2.5×10^{-3} dpa/s, and the maximum radiation damage was 5 dpa with a total fluence of 1×10^{15} ions/cm^2.

3. Results

Fig. 1 demonstrates the texture analysis of as-deposited Cu and $Cu_{97}Fe_3$ films. The conventional two-theta scans in Fig. 1(a) show that both films are highly {111} textured. The Phi scans in Fig. 1(b) show the diffraction peaks from both twin and matrix orientations with nearly identical intensity, indicating the formation of significant growth twin structures.

Fig. 2 compares the microstructural evolution of NT-Cu and $Cu_{97}Fe_3$. Cross-section TEM micrographs show that nanotwins in Cu have a smaller average twin spacing, ~5 nm, comparing with ~14 nm for the NT-$Cu_{97}Fe_3$. The twin spacing here is defined as the distance between two adjacent CTBs [57]. No obvious TB migrations were observed during the annealing process at 200 °C for 30 min.

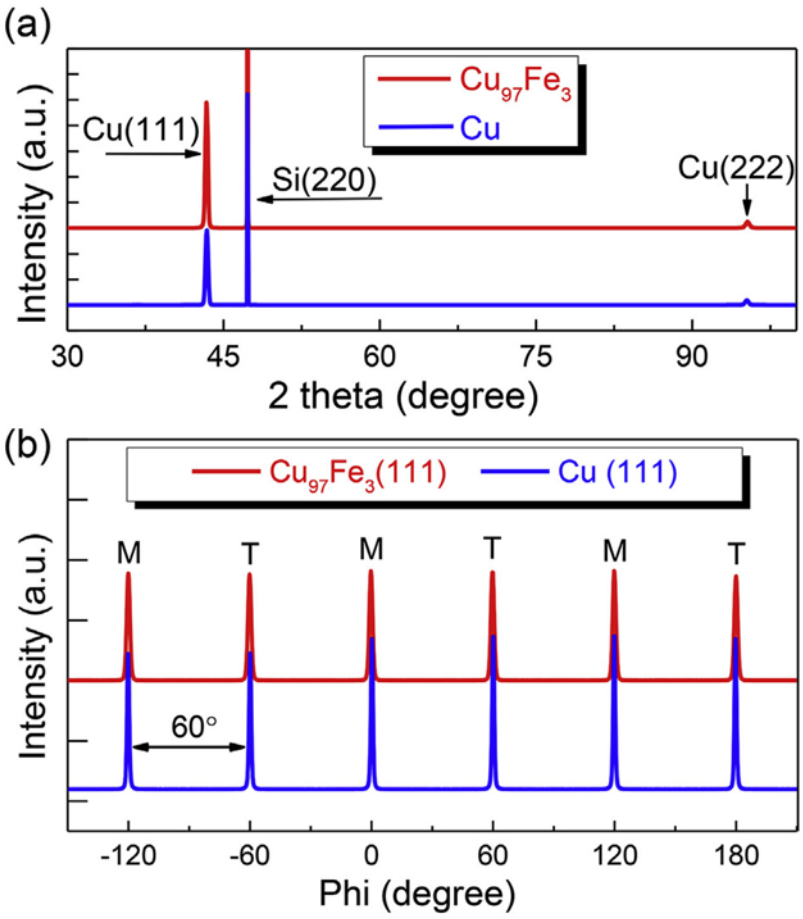

Fig. 1. Texture analysis of XRD profiles of sputtered Cu (blue) and $Cu_{97}Fe_3$ films (red) on Si (110) substrates. (a) Two-theta scans showing strong (111) texture along growth direction for both films. (b) Phi-scan profiles with a six-fold symmetry, indicating a significant fraction of twins in both Cu and $Cu_{97}Fe_3$ films. M and T denote three matrix and twin peaks, respectively.

However, once radiation started, detwinning took place in NT-Cu, giving rise to significant increase in twin spacing, as shown in Fig. 2(a1-a4). In contrast, nanotwins in NT-$Cu_{97}Fe_3$ exhibited superior stability, and most of TBs survived after irradiation to 5 dpa, as shown in Fig. 2(b1-b4). See supplementary video SV1 for more details. Statistical studies in Fig. 2(c1) and (c2) show the irradiation-induced prominent increase of average twin spacing (λ_{ave}) in NT-Cu from 5 to 29 nm (after 5 dpa), while the λ_{ave} in NT-$Cu_{97}Fe_3$ increased slightly from 14 to 16 nm.

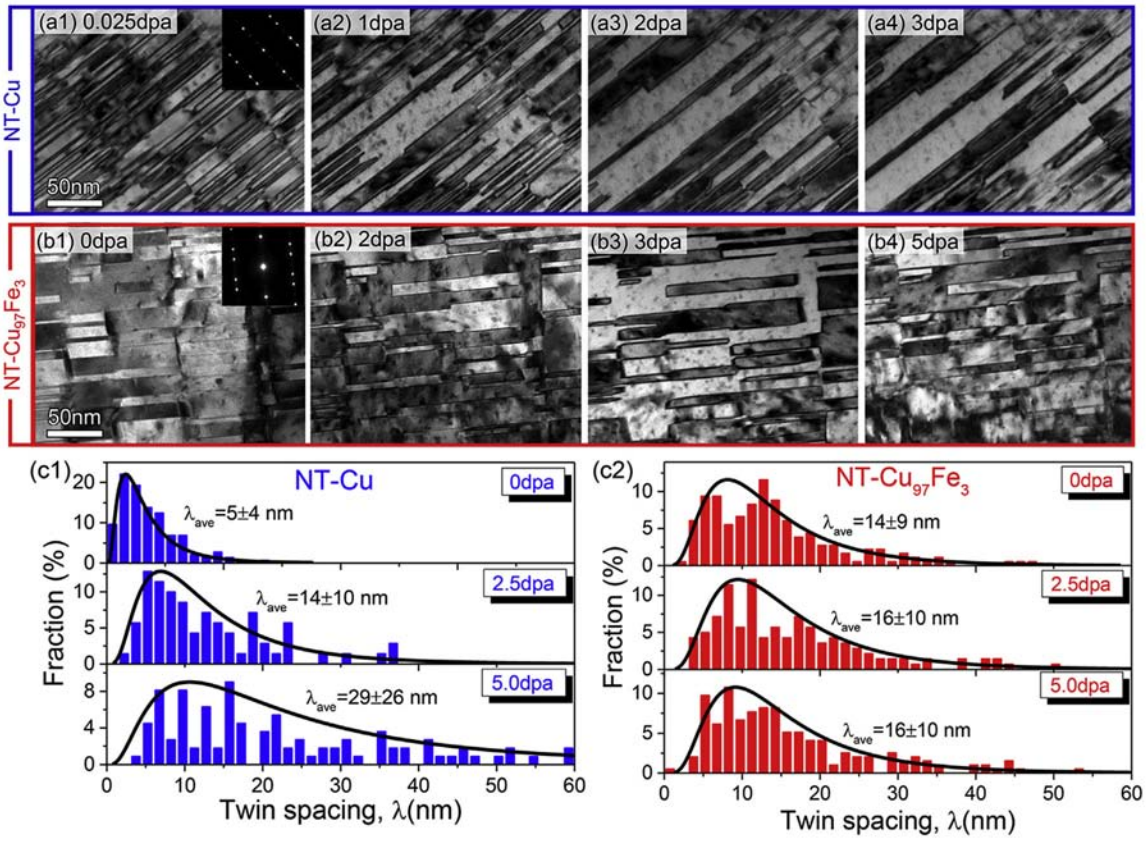

Fig. 2. Evolution of nanotwins in NT-Cu and NT-$Cu_{97}Fe_3$ under Kr^{++} irradiation at 200 °C. (a1-a4) Irradiation-induced significant decrease of twin density in NT-Cu. (b1-b4) Superior stability of nanotwins against irradiation in NT-$Cu_{97}Fe_3$ to 5 dpa. (c1-c2) Statistical distributions show that the average twin spacing (λ_{ave}) of irradiated NT-Cu increases significantly from 5 to 29 nm, whereas the λ_{ave} in NT-$Cu_{97}Fe_3$ increases slightly from 14 to 16 nm. See supplementary video SV1 for more details.

The irradiation-induced detwinning event is attributed to defect-TB interactions. **Fig. 3** compares the irradiation response of CTBs. It has been found that CTBs can become curved to accommodate defect clusters formed in the vicinity. Since defect clusters are often small and have transient lifetime [62,74], they introduce local and temporary distortion (in form of curvatures) along CTBs. As shown in Fig. 3, the local curved CTBs were frequently observed in both cases and they exhibited surprising resilience and self-healing ability. In NT-Cu at ~1.8 dpa in Fig. 3(a1), the CTBs appeared straight. After 6 s in Fig.

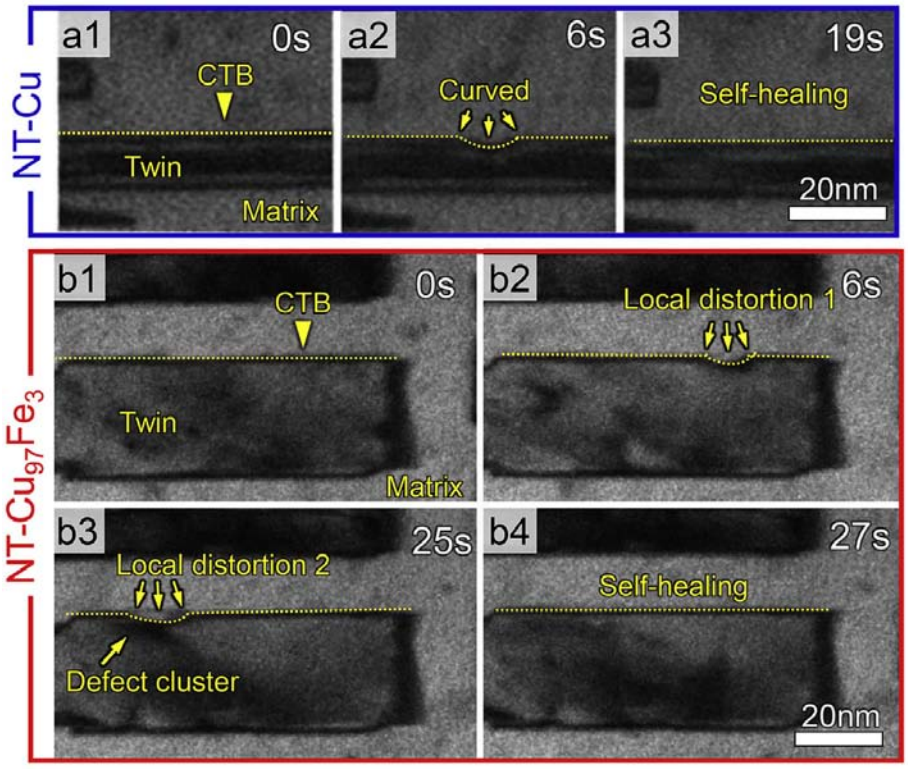

Fig. 3. Local distortion and self-healing capacity of CTBs in NT-Cu (a1-a3) and NT-$Cu_{97}Fe_3$ (b1-b4). See supplementary videos of SV2 and SV3 for more details.

3(a2), the CTB became curved. However, by 19 s in Fig. 3(a3), the distorted CTB had recovered and restored its straight appearance. Similarly, in NT-$Cu_{97}Fe_3$, the upper CTB appeared straight initially (~2.5 dpa) in Fig. 3(b1). At 6 s in Fig. 3(b2), a local distortion was identified at position 1. By 25 s in Fig. 3(b3), the distortion 1 had recovered, while a new distortion at position 2 occurred due to the interaction between the CTB and a defect cluster. At 27 s in Fig. 3(b4), the distortion 2 also recovered. More detailed information can be found in supplementary videos of SV2 and SV3.

By comparison, the ITBs in irradiated NT-Cu frequently migrated and showed prominent thickness-dependence. When the twin thickness (t) is several nanometers, ITBs migrate drastically. As shown in **Fig. 4**(a), an ultrafine twin (3 nm in thickness) was 79 nm long at 0 s (~0.1 dpa). At 2 s in Fig. 4(b), its ITB migrated abruptly by 38 nm. By 10 s in Fig. 4(c), the twin had fully retracted (disappeared). More detailed information can be found in Supplementary Video SV4.

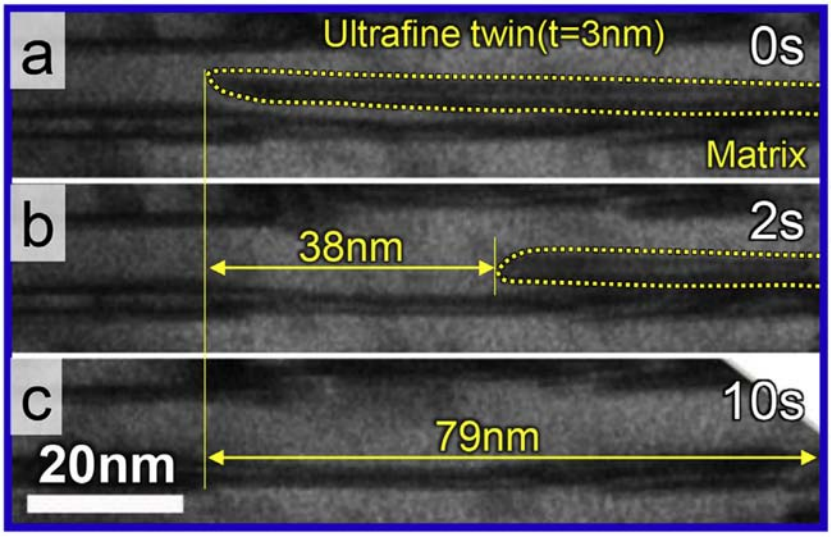

Fig. 4. The drastic ITB migration of an ultrafine twin (~3 nm in thickness) in NT-Cu. See supplementary video SV4.

However, when t > 10 nm, ITB migration often starts from twin corners. As shown in **Fig. 5**(a1) at ~ 3.1 dpa, T_1 (t_1 = 13 nm) had a vertical ITB with two right corners. In 65 s in Fig. 5(a2), the lower right corner retracted leftward by 10 nm and continued to retract by 13 nm after 69 s in Fig. 5(a3). Meanwhile, the upper corner experienced detwinning by 6 nm by 65 s, and recovery by 76 s as shown in Fig. 5(a4). With further irradiation to 126 s, both corners retracted by 14 nm and 20 nm, respectively, leading to a sharp tip in the middle of the ITB as shown in Fig. 5(a5). The protrusion remained unchanged, until significant detwinning occurred instantaneously at 160 s in Fig. 5(a6).

By comparison, the ITBs in NT-$Cu_{97}Fe_3$ remained stable regardless of twin thickness. For instance, three typical twins (T2, T3 and T4) with various thickness were monitored during irradiation (2.4–2.8 dpa) as shown in Fig. 5(b1-b6). No ITB migration was observed, even for the ultrafine twin T2 (t_2 = 3 nm). Note that the ITB of T3 (t_3 = 12 nm), as shown in the box in Fig. 5(b1), was initially sharp, but subsequently dissociated into a 3-nm-wide diffuse ITB after 98 s in Fig. 5(b4). The diffuse ITB extended further to be 4 nm wide, as shown in Fig. 5(b6). T4 (t_4 = 27 nm) has a diffuse ITB, which is 7 nm wide and its width remained unchanged during irradiation. The diffuse ITB absorbed a large defect cluster, an SFT in its vicinity, as shown in Fig. 5(b2-b3). Meanwhile, CTBs also actively engaged in absorbing defects and became

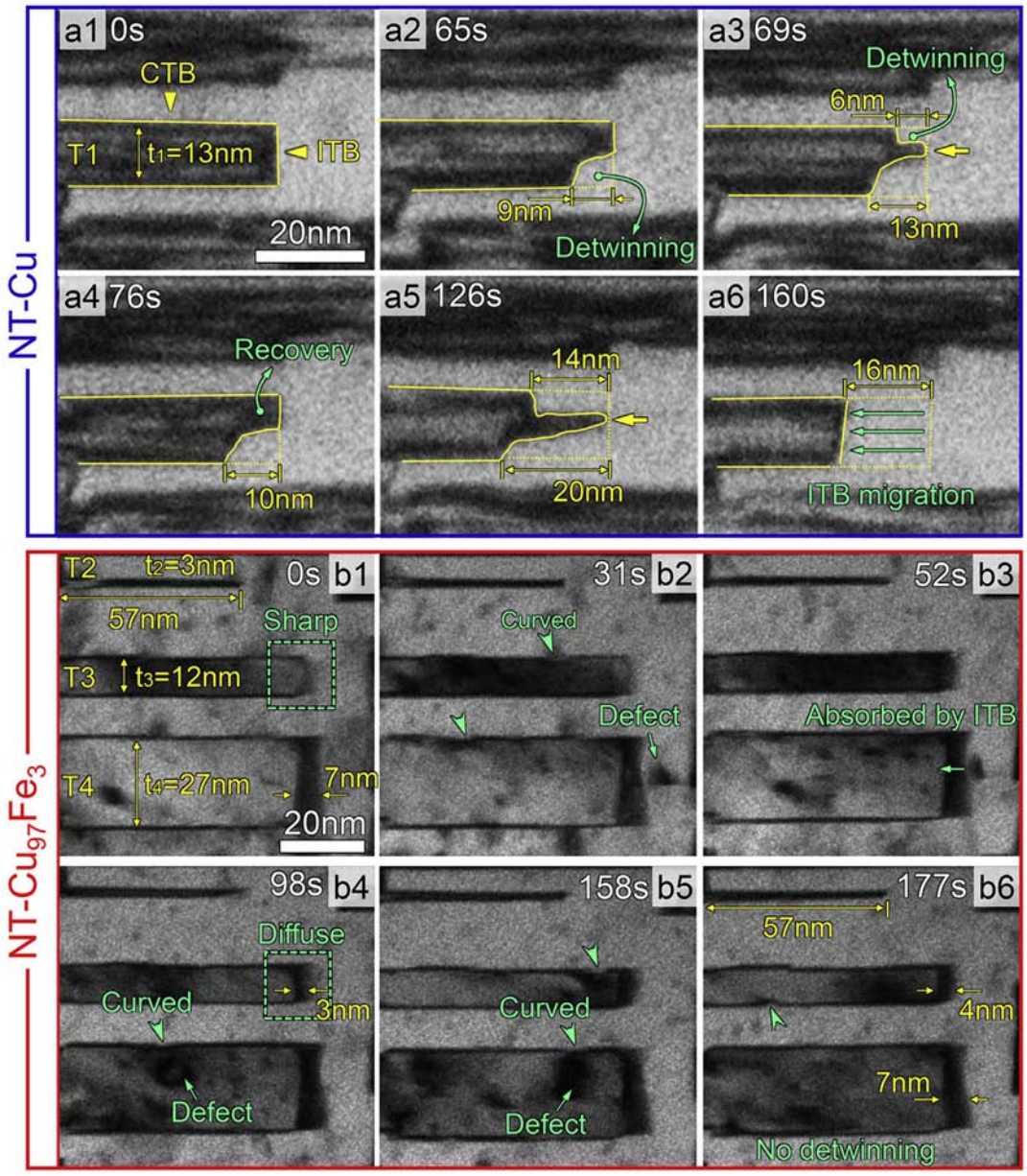

Fig. 5. *In-situ* TEM snapshots comparing the distinct irradiation responses of ITBs between NT-Cu and NT-$Cu_{97}Fe_3$. (a1-a6) The gradual ITB migration and detwinning of T1 (t_1 = 13 nm) in NT-Cu (3.1–3.5 dpa). (b1-b6) The stability of TBs against irradiation (2.4–2.8 dpa) in NT-$Cu_{97}Fe_3$. No detwinning was observed regardless of twin thickness. See supplementary videos SV5 and SV6 for more details.

curved locally, as marked by the green arrows in Fig. 5(b2-b6). More details related to the irradiation responses of ITBs in NT-Cu and NT-$Cu_{97}Fe_3$ can be found in supplementary videos SV5 and SV6.

High-resolution TEM (HRTEM) experiments were performed to examine the evolution of TBs in irradiated NT-Cu and NT-$Cu_{97}Fe_3$ along <110> zone axis. Before irradiation, as shown in **Fig. 6**(a1) and (b1), the CTBs are sharp, and the ITB width is narrow, ~1 nm in both systems. After irradiation to 5 dpa, numerous stacking faults (SFs) emerged in NT-Cu along CTBs, and the thickness of SF ribbon is ~2 nm, whereas the thickness of CTBs in irradiated NT-$Cu_{97}Fe_3$ increases slightly in Fig. 6(b2). The ITBs of irradiated NT-Cu remain narrow (~1 nm), while the irradiated ITBs in NT-$Cu_{97}Fe_3$ have dissociated into a slab bounded by two curved phase boundaries. A typical example of the dissociated ITB in NT-$Cu_{97}Fe_3$ is shown in Fig. 6(b2). The lower-left

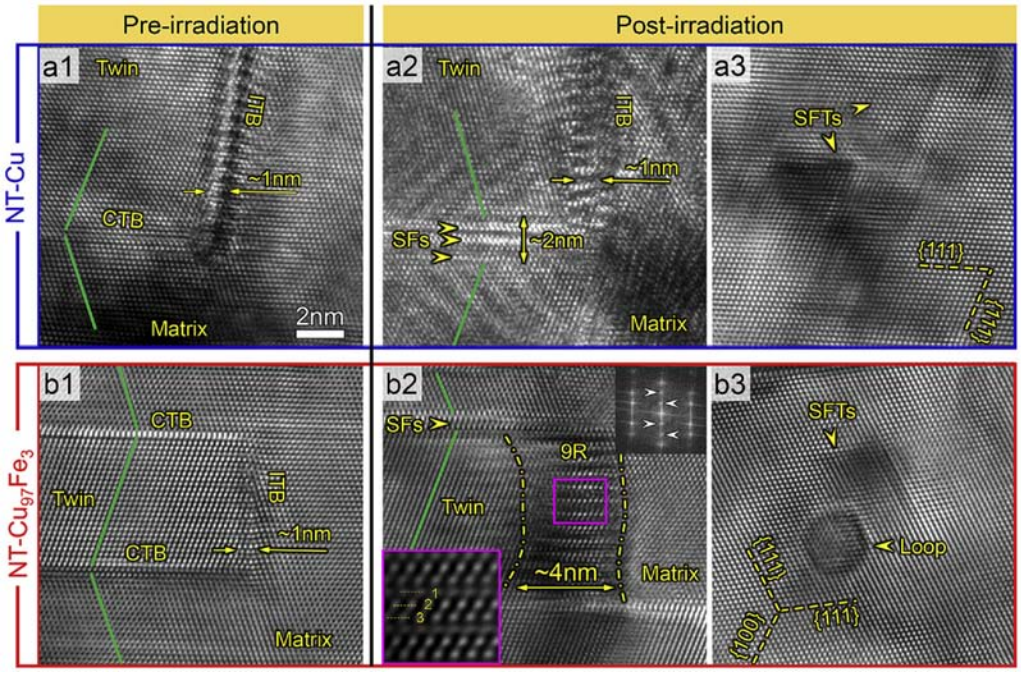

Fig. 6. HRTEM micrographs of TBs and irradiation-induced defects in NT-Cu and NT-$Cu_{97}Fe_3$ before and after irradiation (5 dpa). (a1) and (b1) TBs are sharp in both systems prior to irradiation. (a2) In irradiated NT-Cu, ITBs remain sharp, but CTBs are decorated with SF ribbons. (a3) Irradiation-induced triangular SFTs in NT-Cu. (b2) Radiation of NT-Cu97Fe3 induces broad ITBs, identified as 9R; but CTBs remain largely unchanged. (b3) The irradiated NT-$Cu_{97}Fe_3$ contains SFTs and prismatic dislocation loops.

inset shows that the dissociated ITB region has a repeatable pattern, identified as 9R phase, which is also confirmed by the inserted fast Fourier transform (FFT). Note that in Fig. 5(b6) the dissociated ITB region of T4 is wider than that of T3, and it appears that the width of dissociated ITBs varies with twin thickness as will be shown later. HR-TEM images in Fig. 6(a3) and (b3) also reveal that the defect clusters in NT-Cu are dominated by high-density triangular SFTs, whereas the defects in NT-Cu include SFTs and prismatic dislocation loops.

In-situ TEM technique permits the determination of ITB migration velocity (V_{ITB}). **Fig. 7**(a) indicates that irradiation induces ITB migration in NT-Cu, and the V_{ITB} decreases with increasing thickness (*t*). Moreover, V_{ITB} of NT-Cu increases significantly with increasing irradiation temperature (to 200 °C). In contrast, the ITBs in NT-$Cu_{97}Fe_3$ barely migrate during irradiation at 200 °C. In addition, Fig. 7(b) illustrates that the ITB width (W_{ITB}) of irradiated NTCu has little variation and remains ~1 nm. In comparison, the W_{ITB} of irradiated NT-$Cu_{97}Fe_3$ elevates with increasing *t*, ranging from 3 to 10 nm.

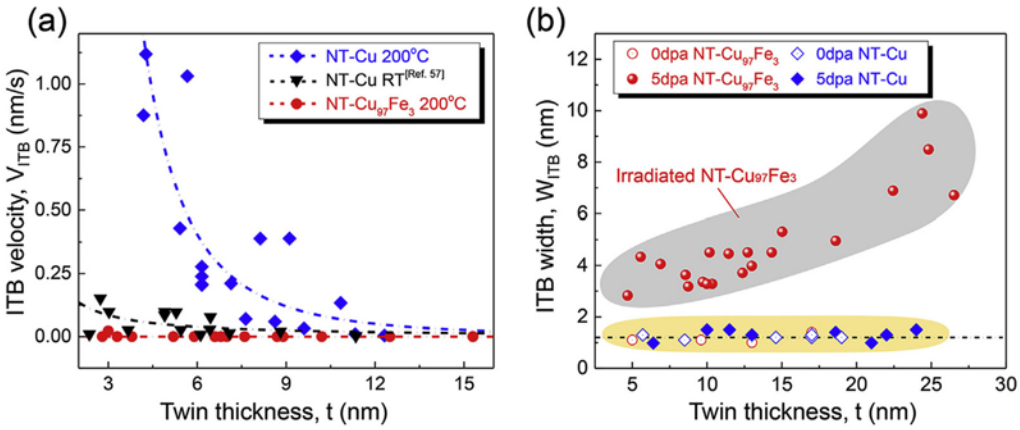

Fig. 7. Irradiation-induced evolution of ITB velocity (V_{ITB}) and width (W_{ITB}), plotted as a function of twin thickness (*t*) for NT-Cu and NT-$Cu_{97}Fe_3$. (a) V_{ITB} increases rapidly with decreasing twin thickness for NT-Cu or at higher irradiation temperature. A reference black data set of NT-Cu irradiated at room temperature (RT) is also plotted [57]. The V_{ITB} is extremely low and barely changes for NT-$Cu_{97}Fe_3$ even for finest twins (t < 5 nm). (b) W_{ITB} of NT-Cu remains constant, ~1 nm, after radiation. However, the W_{ITB} of the irradiated NT-$Cu_{97}Fe_3$ increases monotonically with *t*.

4. Discussion

4.1. Thickness and temperature dependent detwinning in NT-Cu

Our *in-situ* TEM observations reveal that CTBs exhibit surprising resilience and self-healing ability in response to irradiation, as shown in Fig. 3. This is determined by the nature of irradiation-induced defect clusters and interactions with CTBs. Since defect clusters are often small and have transient lifetime [62,74], they introduce only local and temporary distortion (in form of curvatures) along CTBs. Moreover, previous studies show that the SFTCTB interactions can lead to the formation of multiple SFs [56,74]. This is also confirmed by our post-irradiation HRTEM analysis in Fig. 6(a2) and Fig. 6(b2), which show that CTBs appear 'thicker' after irradiation. Our *in-situ* observations also show that irradiation-induced detwinning occurs primarily through ITB migration. The ITBs in FCC Cu are composed of three types of mobile Shockley partials on successive (111) planes [75–77]. Fig. 8(a1) schematically illustrates the ITB structure, including one pure edge partial (b_1) and two mixed partials (b_2 and b_3). This dislocation model has the advantage of relating ITB structure to its migration or dissociation.

ITBs in pure metals can migrate under shear stress through the collective glide of partials [78,79], known as the phase-boundary-migration (PBM) mechanism [80,81]. Impingement of defect clusters during radiation can enhance TB migration by lowering the activation energy barrier for dislocation glide [82]. Consequently, heavy ion irradiation induces ITB migration and detwinning in NTCu, as shown schematically in Fig. 8(a1-a3). The ITB migration velocity, V_{ITB}, in NT-Cu is closely associated with twin thickness (t). The driving force, $2\gamma_{Twin}/t$, for ITB migration increases with decreasing t [57], and γ_{Twin} is twin boundary energy for S3 {111}, approximately ½ of γ_{SF}, with γ_{SF} being the stacking faulty energy (SFE). When t is comparable to the size of defect clusters, the entire ITB can migrate rapidly (see Fig. 4), and thus a fine twin is more likely to undergo detwinning, as shown in **Fig. 8**(a2-a3). For a thicker twin (t > 10 nm), however, detwinning often starts from twin corners, presumably because the migration of ITBs from corners does not change the total length or energy of the TBs [67]. If this analysis is correct, the reverse process, twinning from corner should also occur when local shear stress reverses its sign. Indeed, this hypothesis has been confirmed by our *in-situ* TEM observations in Fig. 5(a3-a4).

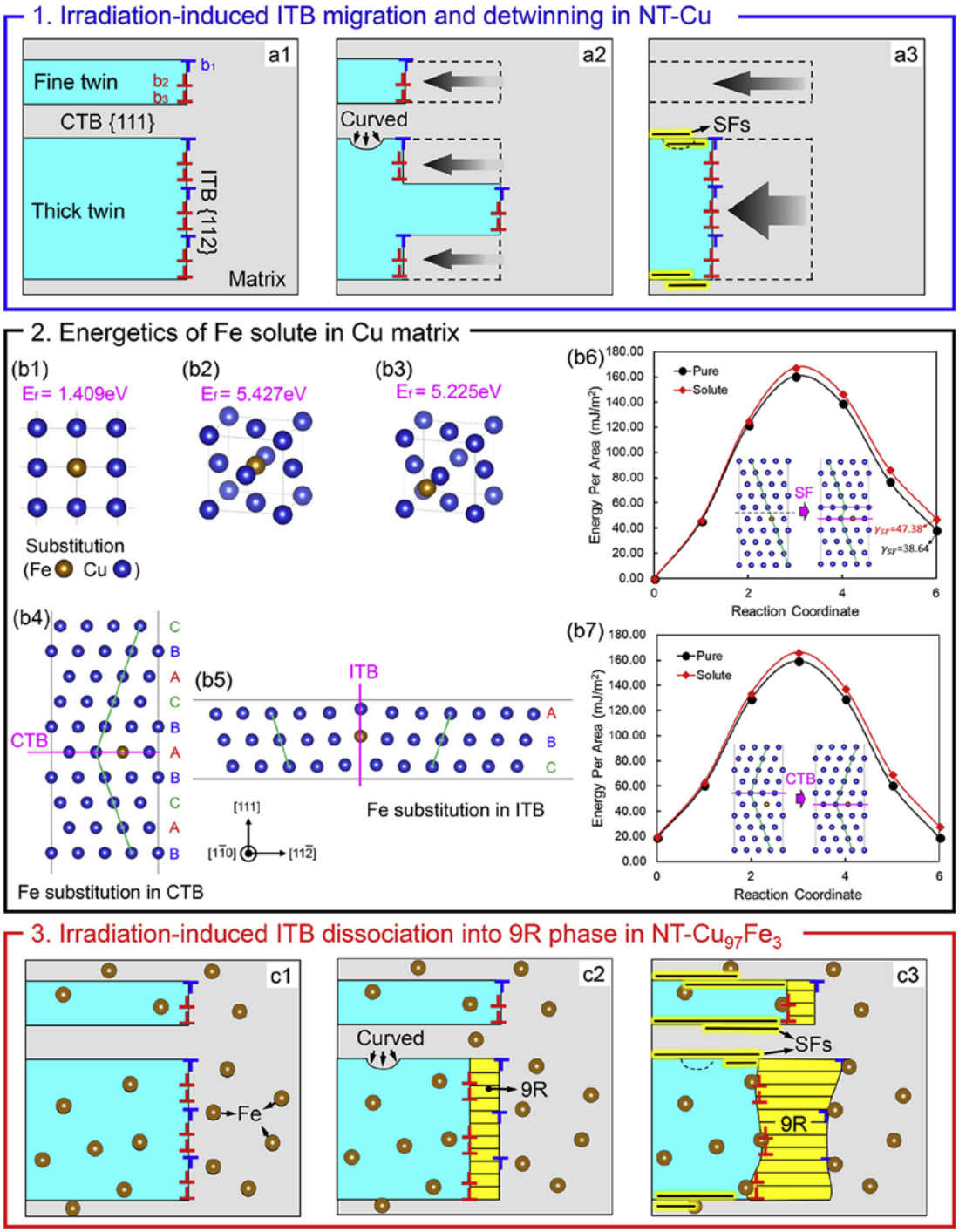

Fig. 8. Irradiation responses of TBs in NT-Cu and NT-$Cu_{97}Fe_3$. (a1-a3) Irradiation-induced ITB migration and detwinning in NT-Cu. (b1-b7) DFT calculations of the energetics of Fe solute in Cu lattice, SF plane, CTB and ITB. (c1-c3) Irradiation of NT-$Cu_{97}Fe_3$ induces dissociation of ITBs into 9R phase, which is pinned by Fe solute atoms, and thus prohibit detwinning. In addition, irradiation can cause CTB distortions in form of curved TBs in both NT-Cu and NT-$Cu_{97}Fe_3$.

At elevated temperatures, the Shockley partials possess higher mobility due to a reduced friction stress, and the driving force for detwinning also increases, and thus the ITB migration velocity increases further in NT-Cu.

4.2. Energetics of Fe solutes in Cu

In-situ studies show that a small amount of Fe solute atoms (~3 at. %) in NT-Cu can significantly enhance TBs stability against irradiation at elevated temperatures. First, there is much less detwinning in the irradiated NT-$Cu_{97}Fe_3$ alloy irrespective of original twin thickness (see Fig. 2). Many fine twins survived irradiation, in drastic contrast to the rapid detwinning in NT-Cu. Second, the TB migration velocity in NT-Cu increases sharply with decreasing twin thickness. In the irradiated NT-$Cu_{97}Fe_3$, however, TBs barely migrate. Third, our study shows that ITB migration velocity in NTCu increases significantly during irradiation at elevated temperatures. Irradiation of NT-$Cu_{97}Fe_3$ at the same temperature leads to little sign of detwinning.

To understand the influence of Fe on TB stability, we examined the energetics of Fe solute in Cu lattice with respect to their locations according to density functional theory (DFT) calculations. The detailed calculation procedure can be found in the Supplementary Information. The results show that the formation energy (E_f) of a single Fe solute is 1.409 eV for substitutional site (Fig. 8(b1)), 5.427 eV for tetrahedral interstitial (Fig. 8(b2)) and 5.225 eV for octahedral interstitial site (Fig. 8(b3)). In comparison, E_f of Cu self-interstitial atom for tetrahedral and octahedral site is 3.901 and 3.488 eV, respectively, much lower than that of Fe interstitial. These results show that Fe solute prefers to stay at substitutional site and can hardly diffuse via interstices. E_f of Fe substitutional pair located at different neighboring sites is also calculated. For the first, second, third, and fourth nearest sites, the formation energies are 2.294, 2.744, 2.805 and 2.766 eV, respectively. E_f of four Fe atoms at nearest substitutional sites is 1.533 eV. Therefore, the segregation of Fe atoms is energetically preferred. But, as mentioned earlier, the diffusion of Fe is energetically difficult, so the Fe solutes are expected to be homogeneously distributed in Cu matrix during deposition, which is consistent with our EDS analysis shown in Supplementary Fig. S2.

The formation energies of Fe solutes at SF plane, CTB (Fig. 8(b4)) and ITB (Fig. 8(b5)) are also calculated. As shown in Fig. 8(b6), the calculated stacking fault energy (γ_{SF}) of pure Cu is 38.64 mJ/m^2. If one of the 16 Cu atoms on a fault plane is replaced by an Fe atom, the stacking fault energy increases to 47.38 mJ/m$_2$. For the model with CTB, the segregation energy of Fe, the energy change for moving Fe atom from defect free crystal to the twin boundary, is 0.048 eV, which suggests that the CTB is not the preferred site for Fe solutes. The energy barrier of CTB migration shown in Fig. 8(b7) increases by adding Fe solutes. In addition, the formation energies of Fe solutes in ITB at substitutional and interstitial sites are 0.623–0.824 eV and 1.669–1.750 eV, respectively. The lower formation energies indicate that ITBs are thermodynamically favorable sites for Fe solutes.

4.3. Mechanisms of irradiation stability of nanotwins in NT-$Cu_{97}Fe_3$

Post-radiation TEM studies in Fig. 6(b2) show that the ITBs in irradiated NT-$Cu_{97}Fe_3$ dissociate into a broad 9R phase, bounded by two phase boundaries. Furthermore, the width of 9R phase increases with increasing twin thickness, as illustrated in Fig. 7(b). Such an observation has profound impact on TB stability and radiation tolerance of irradiated NT Cu–Fe alloys and warrants further discussions.

First, the ITB dissociation occurs through the glide of arrays of Shockley partials [77,83]. When an ITB is subjected to shear, τ_{yx}, the glide force on the partial dislocation b_1 is expressed by Ref. [81]:

$$F_x = -\tau_{yx} b_1 + F_{b_1 b_2} + F_{b_1 b_3} + \gamma_{SF} + F_P \quad (1)$$

The first term on the right in Equation (1) represents the driving force for migration of b_1 under external shear stress. The resistance for the migration of b_1 arises from $F_{b_1 b_2}$ and $F_{b_1 b_3}$, the attractive force between b_1 and b_2 (b_3); the stacking fault energy, γ_{SF}, and the friction force due to Peierls stress, F_P. During irradiation of monolithic NT-Cu, defect clusters will generate a shear stress that drives the migration of ITBs [60]. The γ_{SF} of Cu is low, and F_P is typically negligible in Cu, and thus the resistance to the migration of TB is relatively low.

Our DFT calculations show that Fe can increase the γ_{SF}, consequently the resistance for ITB migration increases substantially in NT

$Cu_{97}Fe_3$ alloys. Also the growth twin density in as-deposited $NTCu_{97}Fe_3$ is lower than that in as-deposited NT-Cu, in agreement with the twin nucleation theory in sputtered films that suggests a higher γ_{SF} leads to a lower probability of twin nucleation [51]. Moreover, post-radiation TEM studies show that a majority of defect clusters in irradiated NT-Cu are SFTs; however, both SFTs and large prismatic dislocation loops are observed in irradiated $NTCu_{97}Fe_3$ alloy. Prismatic loops are often observed in irradiated materials with higher γ_{SF} [84].

Second, it has been shown in monolithic NT metals, that the edge Shockley partial and two mixed partials migrate together due to their mutual attractive forces [81]. MD simulations have shown that the edge partial, b_1, tends to migrate first under shear. The attractive force between b_1 and b_2 (b_3) then drags the two mixed partials to move together, leading to the migration of ITBs. The current study shows that radiation of NT-Cu did not change the width of ITBs, ~ 1 nm. However, the width of ITBs in irradiated $NTCu_{97}Fe_3$ increases rapidly during irradiation to 3–10 nm. Thus, the attractive force between b_1 and b_2 (b_3) decreases, making the migration of ITBs difficult. Previous *in-situ* TEM studies showed that broad 9R in twinned Ag is unstable, and can "zip" together into a sharp ITB under e-beam irradiation to relax internal stress, and migrates rapidly thereafter [83]. As the 9R phase is stabilized by Fe solute and remains broad in the irradiated NT-$Cu_{97}Fe_3$, its migration becomes difficult.

Third, our *in-situ* radiation studies in Fig. 5(b1-b6) show that 9R phase in NT $Cu_{97}Fe_3$ is an excellent defect sink, as it can capture and absorb defect clusters, such as dislocation loops and SFTs. Consequently, the 9R phase becomes broader, as schematically shown in Fig. 8(c2). Since thicker twins have greater probability to capture defect clusters [74], the width of their 9R increases with twin thickness, as shown in Fig. 8(c3). 9R and CTBs can thus form an effective defect-sink network, contributing to the remarkable radiation tolerance of NT-$Cu_{97}Fe_3$ alloy.

The dissociation of an ITB into 9R phase has been reported in pure Au [85], Ag [86] and Cu [76] with low γ_{SF} [87]. It has been concluded that the degree to which ITBs dissociate depends not only on the local stress state within specimen but also on the stacking fault energy [88]. Our study suggests that using appropriate solutes may effectively stabilize 9R phase in various metallic materials. Recently, high-density

9R phase has also been reported in sputtered NT Al-Fe [89], Al-Ti [90] and Al-Mg [91] solid solution alloys. These studies reveal that 9R phase is also beneficial for improving the mechanical properties (high strength and plasticity) of NT metals. The current study suggests that 9R phase coupled with the selection of appropriate solutes may significantly enhance the radiation resistance and stability of nanotwins in a broad range of metallic materials.

5. Conclusions

Nanotwinned Cu and Cu97Fe3 were *in-situ* irradiated using Kr^{++} at 200 °C under the same condition inside a transmission electron microscope. Monolithic NT-Cu experiences prominent detwinning through ITB migration, whereas the nanotwins in NT-$Cu_{97}Fe_3$ alloy remain stable. The outstanding radiation and thermal stability of TBs in NT-$Cu_{97}Fe_3$ arise from the dissociation of ITBs into a broad 9R phase, which also actively absorbs radiation-induced defects. The enhanced twin stability is also attributed to the drag effect of Fe solutes on the dissociated ITBs. These findings provide an important step forward towards the design of stable radiation-resistant nanotwinned alloys under extreme environments.

Acknowledgments — We acknowledge primary financial support by NSF-CMMI-MOM Program under grant no. 1728419. The work on fabrication of nanotwinned metals is supported by DOE-BES under grant no. DESC0016337. We also thank Peter M. Baldo and Edward A. Ryan at Argonne National Laboratory for their help during *in-situ* radiation experiments. The IVEM facility at Argonne National Laboratory is supported by DOE-Office of Nuclear Energy. Accesses to the Microscopy Centers at Purdue University and the DOE Center for Integrated Nanotechnologies managed by Los Alamos National Laboratory is also acknowledged. D. Y. Xie and J. Wang acknowledge the support by the Nebraska Center for Energy Sciences Research, University of Nebraska–Lincoln. Atomistic simulations were completed utilizing the Holland Computing Center of the University of Nebraska, which receives support from the Nebraska Research Initiative. We also acknowledge the support by Center for Nanoscale Materials (CNM) at Argonne National Laboratory under CNM Proposal 52081.

Appendix A. Supplementary data to this article follows the References.

Supplemental video files are attached to the main record in this archive (https://digitalcommons.unl.edu).

References

[1] J. Silcox, P. Hirsch, Dislocation loops in neutron-irradiated copper, Phil. Mag. 4 (48) (1959) 1356–1374.

[2] S. Zinkle, R. Sindelar, Defect microstructures in neutron-irradiated copper and stainless steel, J. Nucl. Mater. 155 (1988) 1196–1200.

[3] B.D. Wirth, How does radiation damage materials? Science 318 (5852) (2007) 923–924.

[4] C.J. Ulmer, A.T. Motta, M.A. Kirk, In situ ion irradiation of zirconium carbide, J. Nucl. Mater. 466 (2015) 606–614.

[5] M. Jenkins, Characterisation of radiation-damage microstructures by TEM, J. Nucl. Mater. 216 (1994) 124–156.

[6] S. Zinkle, G. Kulcinski, R. Knoll, Microstructure of copper following high dose 14-MeV Cu ion irradiation, J. Nucl. Mater. 138 (1) (1986) 46–56.

[7] M. Jenkins, A weak-beam electron microscopy analysis of defect clusters in heavy-ion irradiated silver and copper, Phil. Mag. 29 (4) (1974) 813–828.

[8] W. Sigle, M. Jenkins, J. Hutchison, Determination of the nature of stacking-fault tetrahedra in electron-irradiated silver by high-resolution structural imaging, Phil. Mag. Lett. 57 (5) (1988) 267–271.

[9] S. Kojima, Y. Satoh, H. Taoka, I. Ishida, T. Yoshiie, M. Kiritani, Confirmation of vacancy-type stacking fault tetrahedra in quenched, deformed and irradiated face-centred cubic metals, Philos. Mag. A 59 (3) (1989) 519–532.

[10] C. Lu, K. Jin, L. K. Béland, F. Zhang, T. Yang, L. Qiao, Y. Zhang, H. Bei, H.M. Christen, R.E. Stoller, Direct observation of defect range and evolution in ion-irradiated single crystalline Ni and Ni binary alloys, Sci. Rep. 6 (2016).

[11] J. Li, C. Fan, J. Ding, S. Xue, Y. Chen, Q. Li, H. Wang, X. Zhang, In situ heavy ion irradiation studies of nanopore shrinkage and enhanced radiation tolerance of nanoporous Au, Sci. Rep. 7 (2017).

[12] S.J. Zinkle, K. Farrell, Void swelling and defect cluster formation in reactor-irradiated copper, J. Nucl. Mater. 168 (3) (1989) 262–267.

[13] B. Singh, On the influence of grain boundaries on void growth, Phil. Mag. 28 (6) (1973) 1409–1413.

[14] M. Song, Y. Wu, D. Chen, X. Wang, C. Sun, K. Yu, Y. Chen, L. Shao, Y. Yang, K. Hartwig, Response of equal channel angular extrusion processed ultrafine-grained T91 steel subjected to high temperature heavy ion irradiation, Acta Mater. 74 (2014) 285–295.

[15] C. Sun, S. Zheng, C. Wei, Y. Wu, L. Shao, Y. Yang, K. Hartwig, S. Maloy, S. Zinkle, T. Allen, Superior radiation-resistant nanoengineered austenitic 304L

stainless steel for applications in extreme radiation environments, Sci. Rep. 5 (2015) 7801.

[16] B. Muntifering, S.J. Blair, C. Gong, A. Dunn, R. Dingreville, J. Qu, K. Hattar, Cavity evolution at grain boundaries as a function of radiation damage and thermal conditions in nanocrystalline nickel, Materials Research Letters 4 (2) (2016) 96–103.

[17] J. Li, C. Fan, Q. Li, H. Wang, X. Zhang, In situ studies on irradiation resistance of nanoporous Au through temperature-jump tests, Acta Mater. 143 (2017) 30–42.

[18] D. Chen, N. Li, D. Yuryev, J.K. Baldwin, Y. Wang, M.J. Demkowicz, Self-organization of helium precipitates into elongated channels within metal nanolayers, Science Advances 3 (11) (2017).

[19] C. Cawthorne, E. Fulton, Voids in irradiated stainless steel, Nature 216 (5115) (1967) 575–576.

[20] C. Chen, The shapes of irradiation-produced voids in nickel, Phys. Status Solidi 16 (1) (1973) 197–210.

[21] D. Chen, N. Li, D. Yuryev, J.K. Baldwin, Y. Wang, M.J. Demkowicz, Self-organization of helium precipitates into elongated channels within metal nanolayers, Science Advances 3 (11) (2017) eaao2710.

[22] W. Xu, Y. Zhang, G. Cheng, W. Jian, P.C. Millett, C.C. Koch, S.N. Mathaudhu, Y. Zhu, In-situ atomic-scale observation of irradiation-induced void formation, Nat. Commun. 4 (2013) 2288.

[23] C. Du, S. Jin, Y. Fang, J. Li, S. Hu, T. Yang, Y. Zhang, J. Huang, G. Sha, Y. Wang, Ultrastrong nanocrystalline steel with exceptional thermal stability and radiation tolerance, Nat. Commun. 9 (1) (2018) 5389.

[24] S. Zinkle, 1.03-Radiation-Induced Effects on Microstructure, Comprehensive Nuclear Materials, Elsevier, Oxford, 2012, pp. 65–98.

[25] G.S. Was, Fundamentals of Radiation Materials Science: Metals and Alloys, Springer, 2016.

[26] Z. Shang, J. Li, C. Fan, Y. Chen, Q. Li, H. Wang, T. Shen, X. Zhang, In situ study on surface roughening in radiation-resistant Ag nanowires, Nanotechnology 29 (21) (2018) 215708.

[27] X. Zhang, K. Hattar, Y. Chen, L. Shao, J. Li, C. Sun, K. Yu, N. Li, M.L. Taheri, H. Wang, Radiation damage in nanostructured materials, Prog. Mater. Sci. 96 (2018) 217–321.

[28] S. Zinkle, G. Kulcinski, L. Mansur, Radiation-enhanced recrystallization in copper alloys, J. Nucl. Mater. 141 (1986) 188–192.

[29] X. Zhang, K. Hattar, Y. Chen, L. Shao, J. Li, C. Sun, K. Yu, N. Li, M.L. Taheri, H. Wang, Radiation damage in nanostructured materials, Prog. Mater. Sci. 96 (2018) 217–321.

[30] G. Ackland, Controlling radiation damage, Science 327 (5973) (2010) 1587–1588.

[31] I. Beyerlein, A. Caro, M. Demkowicz, N. Mara, A. Misra, B. Uberuaga, Radiation damage tolerant nanomaterials, Mater. Today 16 (11) (2013) 443–449.

[32] M. Demkowicz, R. Hoagland, J. Hirth, Interface structure and radiation damage resistance in Cu-Nb multilayer nanocomposites, Phys. Rev. Lett. 100 (13) (2008) 136102.

[33] A. Misra, M. Demkowicz, X. Zhang, R. Hoagland, The radiation damage tolerance of ultra-high strength nanolayered composites, JOM (J. Occup. Med.) 59 (9) (2007) 62–65.

[34] M. Demkowicz, P. Bellon, B. Wirth, Atomic-scale design of radiation-tolerant nanocomposites, MRS Bull. 35 (12) (2010) 992–998.

[35] Y. Chen, K.Y. Yu, Y. Liu, S. Shao, H. Wang, M. Kirk, J. Wang, X. Zhang, Damage-tolerant nanotwinned metals with nanovoids under radiation environments, Nat. Commun. 6 (2015).

[36] N. Li, M. Demkowicz, N. Mara, Y. Wang, A. Misra, Hardening due to interfacial He bubbles in nanolayered composites, Materials Research Letters 4 (2) (2016) 75–82.

[37] A. Vattré, T. Jourdan, H. Ding, M.C. Marinica, M.J. Demkowicz, Non-random walk diffusion enhances the sink strength of semicoherent interfaces, Nat. Commun. 7 (2016) 10424.

[38] M.J. Demkowicz, R.G. Hoagland, J.P. Hirth, Interface structure and radiation damage resistance in Cu-Nb multilayer nanocomposites, Phys. Rev. Lett. 100 (13) (2008) 136102.

[39] K. Yu, Y. Chen, J. Li, Y. Liu, H. Wang, M.A. Kirk, M. Li, X. Zhang, Measurement of heavy ion irradiation induced in-plane strain in patterned face-centered-cubic metal films: an in situ study, Nano Lett. 16 (12) (2016) 7481–7489.

[40] X.-M. Bai, A.F. Voter, R.G. Hoagland, M. Nastasi, B.P. Uberuaga, Efficient annealing of radiation damage near grain boundaries via interstitial emission, Science 327 (5973) (2010) 1631–1634.

[41] M. Rose, A. Balogh, H. Hahn, Instability of irradiation induced defects in nanostructured materials, Nucl. Instrum. Methods Phys. Res. Sect. B Beam Interact. Mater. Atoms 127 (1997) 119–122.

[42] K. Yu, Y. Liu, C. Sun, H. Wang, L. Shao, E. Fu, X. Zhang, Radiation damage in helium ion irradiated nanocrystalline Fe, J. Nucl. Mater. 425 (1) (2012) 140–146.

[43] G. Cheng, W. Xu, Y. Wang, A. Misra, Y. Zhu, Grain size effect on radiation tolerance of nanocrystalline Mo, Scripta Mater. 123 (2016) 90–94.

[44] T.D. Shen, S. Feng, M. Tang, J.A. Valdez, Y. Wang, K.E. Sickafus, Enhanced radiation tolerance in nanocrystalline Mg Ga 2 O 4, Appl. Phys. Lett. 90 (26) (2007) 263115.

[45] O. El-Atwani, J. Hinks, G. Greaves, J.P. Allain, S.A. Maloy, Grain size threshold for enhanced irradiation resistance in nanocrystalline and ultrafine tungsten, Materials Research Letters (2017) 1–7.

[46] K. Lu, Stabilizing nanostructures in metals using grain and twin boundary architectures, Nature Reviews Materials 1 (2016) 16019.

[47] D. Kaoumi, A. Motta, R. Birtcher, A thermal spike model of grain growth under irradiation, J. Appl. Phys. 104 (7) (2008) 073525.

[48] S.J. Zinkle, G. Was, Materials challenges in nuclear energy, Acta Mater. 61 (3) (2013) 735–758.

[49] L. Lu, Y. Shen, X. Chen, L. Qian, K. Lu, Ultrahigh strength and high electrical conductivity in copper, Science 304 (5669) (2004) 422–426.

[50] D. Bufford, H. Wang, X. Zhang, High strength, epitaxial nanotwinned Ag films, Acta Mater. 59 (1) (2011) 93–101.

[51] X. Zhang, A. Misra, H. Wang, T. Shen, M. Nastasi, T. Mitchell, J. Hirth, R. Hoagland, J. Embury, Enhanced hardening in Cu/330 stainless steel multilayers by nanoscale twinning, Acta Mater. 52 (4) (2004) 995–1002.

[52] X. Zhang, H. Wang, X. Chen, L. Lu, K. Lu, R. Hoagland, A. Misra, High-strength sputter-deposited Cu foils with preferred orientation of nanoscale growth twins, Appl. Phys. Lett. 88 (17) (2006) 173116.

[53] J. Wang, X. Zhang, Twinning effects on strength and plasticity of metallic materials, MRS Bull. 41 (04) (2016) 274–281.

[54] O. Anderoglu, A. Misra, H. Wang, X. Zhang, Thermal stability of sputtered Cu films with nanoscale growth twins, J. Appl. Phys. 103 (9) (2008) 094322.

[55] X. Zhang, A. Misra, Superior thermal stability of coherent twin boundaries in nanotwinned metals, Scripta Mater. 66 (11) (2012) 860–865.

[56] K. Yu, D. Bufford, C. Sun, Y. Liu, H. Wang, M. Kirk, M. Li, X. Zhang, Removal of stacking-fault tetrahedra by twin boundaries in nanotwinned metals, Nat. Commun. 4 (2013) 1377.

[57] Y. Chen, H. Wang, M. Kirk, M. Li, J. Wang, X. Zhang, Radiation induced detwinning in nanotwinned Cu, Scripta Mater. 130 (2017) 37–41.

[58] C. Fan, Y. Chen, J. Li, J. Ding, H. Wang, X. Zhang, Defect evolution in heavy ion irradiated nanotwinned Cu with nanovoids, J. Nucl. Mater. 496 (2017) 293–300.

[59] J. Li, D. Xie, S. Xue, C. Fan, Y. Chen, H. Wang, J. Wang, X. Zhang, Superior twin stability and radiation resistance of nanotwinned Ag solid solution alloy, Acta Mater. 151 (2018) 395–405.

[60] J. Li, K. Yu, Y. Chen, M. Song, H. Wang, M. Kirk, M. Li, X. Zhang, In situ study of defect migration kinetics and self-healing of twin boundaries in heavy ion irradiated nanotwinned metals, Nano Lett. 15 (5) (2015) 2922–2927.

[61] J. Li, Y. Chen, H. Wang, X. Zhang, In situ studies on twin-thickness-dependent distribution of defect clusters in heavy ion-irradiated nanotwinned Ag, Metall. Mater. Trans. 48 (3) (2017) 1466–1473.

[62] C. Fan, J. Li, Z. Fan, H. Wang, X. Zhang, In situ studies on the irradiation-induced twin boundary-defect interactions in Cu, Metall. Mater. Trans. (2017) 1–9.

[63] D.C. Bufford, Y.M. Wang, Y. Liu, L. Lu, Synthesis and microstructure of electrodeposited and sputtered nanotwinned face-centered-cubic metals, MRS Bull. 41 (4) (2016) 286–291.

[64] I.J. Beyerlein, X. Zhang, A. Misra, Growth twins and deformation twins in metals, Annu. Rev. Mater. Res. 44 (2014) 329–363.

[65] J. Du, Z. Wu, E. Fu, Y. Liang, X. Wang, P. Wang, K. Yu, X. Ding, M. Li, M. Kirk, Detwinning through migration of twin boundaries in nanotwinned Cu films under in situ ion irradiation, Sci. Technol. Adv. Mater. 19:1 (2018) 212-220.

[66] Y. Liu, J. Jian, Y. Chen, H. Wang, X. Zhang, Plasticity and ultra-low stress induced twin boundary migration in nanotwinned Cu by in situ nanoindentation studies, Appl. Phys. Lett. 104 (23) (2014) 231910.

[67] J. Miao, Structure and migration of (112) step on (111) twin boundaries in nanocrystalline copper, J. Appl. Phys. 104 (2008) 113717.

[68] K.-C. Chen, W.-W. Wu, C.-N. Liao, L.-J. Chen, K. Tu, Stability of nanoscale twins in copper under electric current stressing, J. Appl. Phys. 108 (6) (2010), 066103.

[69] K.Y. Yu, D. Bufford, F. Khatkhatay, H. Wang, M.A. Kirk, X. Zhang, In situ studies of irradiation induced twin boundary migration in nanotwinned Ag, Scripta Mater. 69 (2013) 385.

[70] N. Li, J. Wang, Y. Wang, Y. Serruys, M. Nastasi, A. Misra, Incoherent twin boundary migration induced by ion irradiation in Cu, J. Appl. Phys. 113 (2) (2013), 023508.

[71] M. Li, M. Kirk, P. Baldo, D. Xu, B. Wirth, Study of defect evolution by TEM with in situ ion irradiation and coordinated modeling, Phil. Mag. 92 (16) (2012) 2048–2078.

[72] J.F. Ziegler, M.D. Ziegler, J.P. Biersack, SRIM–The stopping and range of ions in matter, Nucl. Instrum. Methods Phys. Res. Sect. B Beam Interact. Mater. Atoms 268 (11) (2010) 1818–1823, 2010.

[73] R.E. Stoller, M.B. Toloczko, G.S. Was, A.G. Certain, S. Dwaraknath, F.A. Garner, On the use of SRIM for computing radiation damage exposure, Nucl. Instrum. Methods Phys. Res. Sect. B Beam Interact. Mater. Atoms 310 (2013) 75–80.

[74] Y. Chen, J. Li, K. Yu, H. Wang, M. Kirk, M. Li, X. Zhang, In situ studies on radiation tolerance of nanotwinned Cu, Acta Mater. 111 (2016) 148–156.

[75] G.H. Campbell, D.K. Chan, D.L. Medlin, J.E. Angelo, C.B. Carter, Dynamic observation of the fcc to 9R shear transformation in a copper Σ= 3 incoherent twin boundary, Scripta Mater. 35 (7) (1996) 837–842.

[76] C.B. Carter, D. Medlin, J. Angelo, M.J. Mills, The 112 Lateral Twin Boundary in FCC Materials, Materials Science Forum, Trans Tech Publ, 1996, pp. 209–212.

[77] J. Wang, O. Anderoglu, J. Hirth, A. Misra, X. Zhang, Dislocation structures of S 3 {112} twin boundaries in face centered cubic metals, Appl. Phys. Lett. 95 (2) (2009), 021908.

[78] N. Li, J. Wang, J. Huang, A. Misra, X. Zhang, Influence of slip transmission on the migration of incoherent twin boundaries in epitaxial nanotwinned Cu, Scripta Mater. 64 (2) (2011) 149–152.

[79] N. Li, J. Wang, X. Zhang, A. Misra, In-situ TEM study of dislocation-twin boundaries interaction in nanotwinned Cu films, J. Occup. Med. 63 (9) (2011) 62–66.

[80] J. Wang, A. Misra, J. Hirth, Shear response of S 3 {112} twin boundaries in face-centered-cubic metals, Phys. Rev. B 83 (6) (2011), 064106.

[81] J. Wang, N. Li, O. Anderoglu, X. Zhang, A. Misra, J. Huang, J. Hirth, Detwinning mechanisms for growth twins in face-centered cubic metals, Acta Mater. 58 (6) (2010) 2262–2270.

[82] D. Song, X. Li, J. Xue, H. Duan, Z. Jin, Irradiation-enhanced twin boundary migration in BCC Fe, Phil. Mag. Lett. 94 (6) (2014) 361–369.

[83] L. Liu, J. Wang, S. Gong, S. Mao, High resolution transmission electron microscope observation of zero-strain deformation twinning mechanisms in Ag, Phys. Rev. Lett. 106 (17) (2011) 175504.

[84] S. Zinkle, L. Seitzman, W. Wolfer, I. Energy calculations for pure metals, Philos. Mag. A 55 (1) (1987) 111–125.

[85] W. Krakow, D.A. Smith, A high-resolution electron microscopy investigation of some low-angle and twin boundary structures, Ultramicroscopy 22 (1–4) (1987) 47–55.

[86] F. Ernst, M.W. Finnis, D. Hofmann, T. Muschik, U. Schönberger, U. Wolf, M. Methfessel, Theoretical prediction and direct observation of the 9R structure in Ag, Phys. Rev. Lett. 69 (4) (1992) 620.

[87] P. Gallagher, The influence of alloying, temperature, and related effects on the stacking fault energy, Metallurgical Transactions 1 (9) (1970) 2429–2461.

[88] D. Medlin, G. Campbell, C.B. Carter, Stacking defects in the 9R phase at an incoherent twin boundary in copper, Acta Mater. 46 (14) (1998) 5135–5142.

[89] Q. Li, S. Xue, J. Wang, S. Shao, A.H. Kwong, A. Giwa, Z. Fan, Y. Liu, Z. Qi, J. Ding, High-strength nanotwinned Al alloys with 9R phase, Adv. Mater. 30 (11) (2018) 1704629.

[90] Y. Zhang, S. Xue, Q. Li, C. Fan, R. Su, J. Ding, H. Wang, H. Wang, X. Zhang, Microstructure and mechanical behavior of nanotwinned AlTi alloys with 9R phase, Scripta Mater. 148 (2018) 5–9.

[91] S. Xue, Q. Li, Z. Fan, H. Wang, Y. Zhang, J. Ding, H. Wang, X. Zhang, Strengthening mechanisms and deformability of nanotwinned AlMg alloys, J. Mater. Res. 33 (22) (2018) 3739–3749.

Appendix A

SUPPORTING INFORMATION

9R phase enabled superior radiation stability of nanotwinned Cu alloys via *in situ* radiation at elevated temperature

Cuncai Fan[a], Dongyue Xie[b], Jin Li[a], Zhongxia Shang[a], Youxing Chen[c], Sichuang Xue[a], Jian Wang[b], Meimei Li[d], Anter El-Azab[a,e], Haiyan Wang[a,f] and Xinghang Zhang[a]*

[a] *School of Materials Engineering, Purdue University, West Lafayette, IN 47907, USA*

[b] *Nebraska Center for Materials and Nanoscience, University of Nebraska-Lincoln, Lincoln, NE 68583-0857, USA*

[c] *Department of Mechanical engineering and engineering science, University of North Carolina, Charlotte, NC 28223-0001, USA*

[d] *Nuclear Engineering Division, Argonne National Laboratory, Argonne, IL 60439, USA*

[e] *School of Nuclear Engineering, Purdue University, West Lafayette, IN 47907, USA*

[f] *School of Electrical and Computer Engineering, West Lafayette, IN 47907, USA*

*Corresponding Author: Xinghang Zhang (xzhang98@purdue.edu)

Supplementary Figures

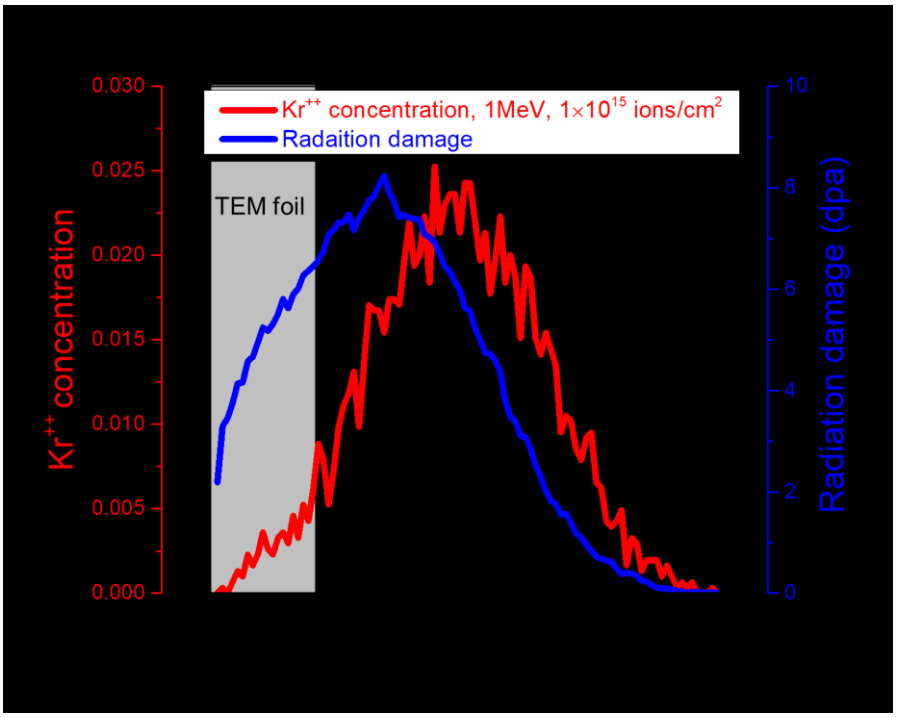

Supplementary Figure S1. (Color online) SRIM simulation showing Kr^{++} concentration (red) and radiation damage (blue) along the ion penetration depth in Cu. For 1 MeV, 1×10^{15} ions/cm^2 Kr^{++}, the calculation reveals that more than 99% Kr^{++} penetrate through the first 100 nm thick TEM foil, leaving behind an average radiation damage of ~ 5 dpa inside the foil.

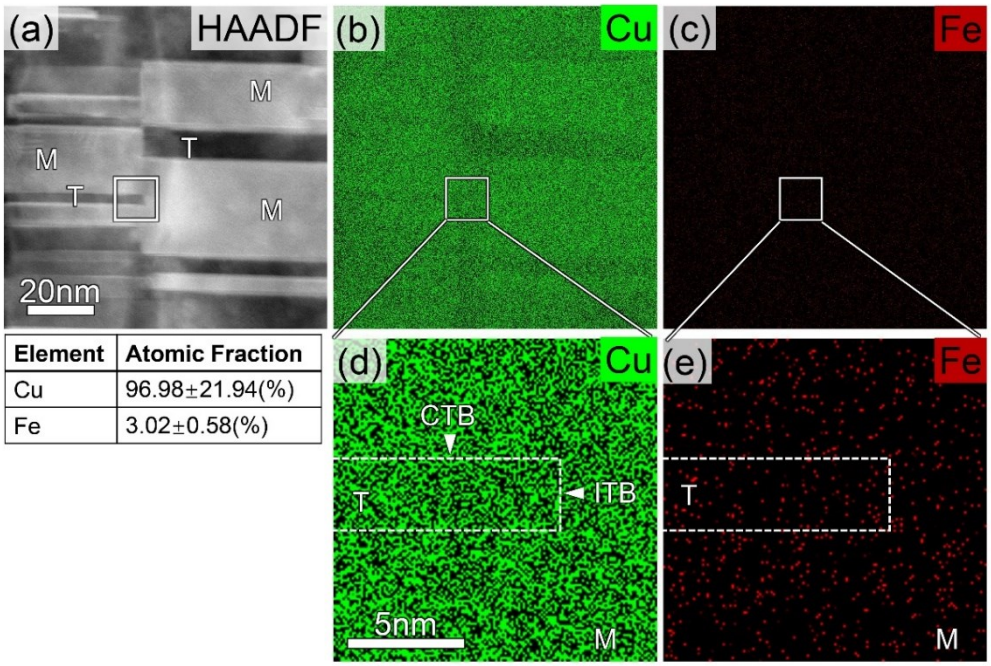

Element	Atomic Fraction
Cu	96.98±21.94(%)
Fe	3.02±0.58(%)

Figure S2. Composition mapping of as-deposited NT-$Cu_{97}Fe_3$. (a) Typical STEM HAADF image of the NT-$Cu_{97}Fe_3$. (b) and (c) corresponding EDS elemental maps of Cu and Fe, respectively. The square box focuses on an ITB. (d) and (e) Enlarged view of the square box showing the uniform distributions of Cu and Fe atoms in twin and matrix.

DFT calculation method

The Vienna ab-initio simulation package (VASP) is used to perform calculation with projector augmented wave (PAW) method[1] and generalized gradient approximation (GGA) approach[2]. During the calculation, spin polarization is considered, and the Perdew-Burke-Ernzerhof (PBE) function[3] is employed. The pseudopotential with electron configuration $3d^{10}4s^{1}$ and $3d^{7}4s^{1}$ is used to describe the behavior of Cu and Fe ion, respectively[4]. The bulk properties are computed with a 3×3×3 supercell containing 106-108 Cu atoms and 0-4 Fe atoms. The slab models for a coherent twin boundary (CTB) and stacking fault (SF) have 10 layers on (111) plane. In each plane, there are 16 atoms. The (112) ITB slab models are constructed with 3 layers on (111) plane and 6 layers on $(\bar{1}10)$ plane. The model contains 104-105 Cu atoms and 1 Fe atom. The first Brillouin zone of bulk models and slab models are sampled with a 3×3×3 and a 4×4×1 M-P k-mesh[5]. A 400eV cut-off energy is used for all calculations in this study. The convergence criteria of geometry optimizations and self-consistent calculations is 0.01eV/Å and 10^{-5}eV respectively. To verify the rationality of parameters used in computations, the properties of copper and iron are calculated with unit cell sampled with a 9×9×9 M-P k-mesh. For copper, the calculated lattice constant is 3.629 Å and the cohesive energy is 3.48 eV. For BCC iron, the lattice constant is 2.2866 Å and the cohesive energy is 4.855 eV. These properties are consistent with previous studies[6-8].

References

[1] P.E. Blöchl, Projector augmented-wave method, Physical review B 50(24) (1994) 17953.
[2] D.C. Langreth, M. Mehl, Beyond the local-density approximation in calculations of ground-state electronic properties, Physical Review B 28(4) (1983) 1809.

[3] J.P. Perdew, K. Burke, M. Ernzerhof, Generalized gradient approximation made simple, Physical review letters 77(18) (1996) 3865.
[4] G. Kresse, D. Joubert, From ultrasoft pseudopotentials to the projector augmented-wave method, Physical Review B 59(3) (1999) 1758.
[5] H.J. Monkhorst, J.D. Pack, Special points for Brillouin-zone integrations, Physical review B 13(12) (1976) 5188.
[6] E. Kaxiras, Atomic and electronic structure of solids, Cambridge University Press2003.
[7] A.W. Hull, A new method of X-ray crystal analysis, Physical Review 10(6) (1917) 661.
[8] E. Owen, E. Yates, XLI. Precision measurements of crystal parameters, The London, Edinburgh, and Dublin Philosophical Magazine and Journal of Science 15(98) (1933) 472-488.

Supplementary Video Captions

Supplementary Video SV1. Comparison of the evolution of twins in NT Cu (left) and NT $Cu_{97}Fe_3$ (right) under Kr^{++} irradiation at 200 ºC up to1.2 dpa. Note that the videos have been accelerated by 16 times.

Supplementary Video SV2. Self-healing of CTBs in irradiated NT-Cu from 1.80 to 1.81 dpa. The video corresponds to the snapshots in Figure 3 (a1-a3).

Supplementary Video SV3. Self-healing of curved CTBs in irradiated NT-$Cu_{97}Fe_3$ from 2.50 to 2.51 dpa. The video corresponds to the snapshots in Figure 3(b1-b4).

Supplementary Video SV4. Drastic ITB migration of an ultrafine twin (~3 nm in thickness) in irradiated NT Cu at ~ 0.1 dpa. The video corresponds to the snapshots in Figure 4.

Supplementary Video SV5. Gradual migration of a long ITB of a thick twin (~13 nm in thickness) in NT-Cu from 3.1 to 3.5 dpa. The video corresponds to the snapshots in Figure 5(a1-a6). Note that the video has been accelerated by 8 times.

Supplementary Video SV6. The absorption of a defect cluster by a diffuse ITB in NT-$Cu_{97}Fe_3$ from 2.4 to 2.8 dpa. The video corresponds to the snapshots in Figure 5(b1-b6).